Internal thermal noise calculation method for KAGRA cradle-mirror system

K. Rainer Corley

Gravitational Wave Project Office, National Astronomical Observatory of Japan,
Osawa 2-21-1, Mitaka, Tokyo, Japan 181-8588

Internal thermal noise in the proposed KAGRA cradle-mirror system is calculated using a finite element application of Levin's direct approach. Internal displacement noise spectra due to the mirror-cradle system, as well as indium separation patches, are calculated individually. The work is used to (1) estimate the necessary value of the loss factor of these indium patches (for the parameters chosen, a value of 1.1×10^{-4} is estimated), and (2) to provide a method for making internal thermal noise calculations for future proposals for the system.

Contents

1 Introduction

Thermal noise is the dominant noise source for interferometric gravitational wave detectors in various frequency ranges, depending on the design of the detector. It is a significant problem for future detector projects, such as the KAGRA project. Calculating the thermal noise generated gives an important contribution to the overall sensitivity of the detector.

KAGRA, the next interferometric gravitational wave detector in Japan, is making new efforts to quiet thermal noise. For example, the mirrors in this detector will be kept at cryogenic temperatures, which will reduce motion. Beyond this, the detector will be located in an underground mine in Kamioka, Japan, where seismic noise sources will be quieted further. These features have not been seen in any past detectors.

Here, we create a finite-element analysis system to estimate internal thermal noise ranges in the proposed mirror-cradle system of KAGRA. A geometry is assumed here, but the parameters are adjustable for calculations of future proposals. Using this modeling, an acceptable loss factor for the indium patches separating the cradle from the mirror is estimated. For the parameters chosen, this loss factor is estimated to be 1.1×10^{-4}

2 Background

The methods used in this study are based on a numerical application of the fluctuation-dissipation theorem derived by Callen and Welton [*1*]. Specifically, we use an application of this theorem developed by Levin [*2*] for calculating internal thermal noise.

2.1 Internal thermal noise

Thermal noise emerges due to thermal agitation in a system. It is essentially the same phenomenon as damping, but in a different domain; damping occurs at excited initial states, and

thermal noise occurs at equilibrium. It can be seen, for example, in electronics, as Johnson-Nyquist noise.

In the case of the mirror-suspension system of a gravitational wave detector, thermal noise appears as random fluctuations in the position of the mirror, which leads to decreased sensitivity in the detector.

There is a useful distinction to be made between internal and suspension thermal noise. Internal thermal noise is the noise generated intrinsically by the mirror. It is caused by the internal damping of the mirror system. Suspension thermal noise is the noise resulting from the suspension system; it is caused by friction in the suspension system. We are interested in calculating the internal thermal noise in a given system. This allows us to see the effects of different designs on sensitivity.

2.2 Fluctuation-dissipation theorem

The fluctuation-dissipation theorem provides a relation between generalized resistance and fluctuations in generalized forces for linear dissipative systems. One formulation of the theorem is

$$S_F(\Omega) = 4k_B T R(\Omega) \tag{1}$$

where $S_F(\Omega)$ is the force noise power spectrum (for a force acting on the system), k_B is Boltzmann's constant, T is the system's temperature, $R(\Omega)$ is the generalized resistance, and Ω is a parameter (in our case, frequency).

This is the most relevant formulation for our purposes. In gravitational wave detectors, thermal noise is most important far from the resonant frequencies of the system; as a result, a spectral density over a range of frequencies is most useful.

In the case of Johnson-Nyquist noise mentioned above, the application is straightforward. One only needs the temperature and electrical resistance of the system to find a power spectrum. The generalized resistance, however, is not as straightforward in other applications. For

mechanical systems, the generalized resistance is the real part of the mechanical impedance, $Z(\Omega)$, defined as

$$Z(\Omega) = \frac{1}{-i\Omega\chi(\Omega)}, \tag{2}$$

where $\chi(\Omega)$ is the mechanical susceptibility. Using this and Equation 1, it can be shown [*3*] that the displacement thermal noise spectrum (substituting f for the parameter Ω) is

$$S_x(f) = \frac{k_B T}{\pi^2 f^2} \left| \mathrm{Re}[\frac{1}{Z(f)}] \right| . \tag{3}$$

For convenience, we will use the inverse of mechanical impedance, called the admittance, $Y(f) = \frac{1}{Z(f)}$. In terms of the readout (displacement) variable, $x(t)$, it can be shown that

$$Y(f) = 2\pi i f x(f)/F(f). \tag{4}$$

Of course, as indicated in Equation 4, the readout variable and the force function must be written in a frequency domain.

2.3 Levin's direct approach

The real part of the admittance, $Y(f)$, must be calculated to find the spectrum in Equation 3. Because the systems considered will be complicated and far from ideal, this admittance must be calculated numerically.

One numerical approach involves, first, decomposing the readout variable into normal modes. These normal modes are simpler to analyze individually with the fluctuation-dissipation theorem. One can calculate the thermal noise spectrum associated with each normal mode and then add the contributions to obtain the combined noise.

There are two main problems with this approach. First, this assumes that the normal modes of the system can be summed incoherently (i.e. their Langevin forces are independent). However, this is true only if the friction is distributed homogeneously across the volume of the

mirror. This is not a safe assumption; for instance, friction at the surface could vary from that at the center in a number of situations.

The second problem is that for a small beam radius (compared to the mirror radius), the sum over modes converges slowly. This requires computing many modes, which is computationally taxing.

Levin's method presents a simple and accurate expression for estimating the thermal noise of a mirror with an incoming laser beam. The fluctuation-dissipation theorem is applied to the readout variable, $x(t)$. The result gives us an expression for the power spectrum in terms of a force amplitude, F_0, and an average power dissipation, W_{diss}.

Specifically, it can be shown that for a mirror with a Gaussian, sinusoidal load of amplitude F_0, the power spectrum of displacement noise is

$$S_x(f) = \frac{2k_B T}{\pi^2 f^2} \frac{W_{\text{diss}}}{{F_0}^2}. \tag{5}$$

A detailed explanation of the use of this method in this work is given in Section 3.1.

3 Method

The displacement thermal noise at 100 Hz is first calculated in an isolated mirror, and the results are compared to previous studies. Then, this method is used to find the displacement noise for the mirror-cradle system. These noise values are compared using numerous adhesive loss factors at 100 Hz.

3.1 Thermal noise calculation method

Levin's method [2] provides an analytical expression for calculating the internal thermal noise in test masses. Suppose that for a given frequency f, an oscillatory pressure of the form

$$P(\vec{r}, t) = F_0 \cos(2\pi f t) f(\vec{r}) \tag{6}$$

is applied to the face of a test mass. F_0 is the total force magnitude and $f(\vec{r})$ is a normalized spatial distribution. If this causes an average dissipation power in the test mass of W_{diss}, then it can be shown that the real part of the admittance is

$$|\,\text{Re}[\frac{1}{Z(f)}]\,|= \frac{2W_{\text{diss}}}{F_0^2}. \tag{7}$$

Using this result with Equation 3, we see that the spectral density, $S_x(f)$, can be found with

$$S_x(f) = \frac{2k_BT}{\pi^2 f^2}\frac{W_{\text{diss}}}{{F_0}^2}, \tag{8}$$

where k_B is Boltzmann's constant and T is the temperature of the mirror.

For homogeneous power dissipation, W_{diss} can be calculated with

$$W_{\text{diss}} = 2\pi f U_{\max}\phi(f), \tag{9}$$

where $U_{\max}$ is the elastic energy of the test mass at its maximum deformation or extension, and $\phi(f)$ is the loss angle of the material.

In this approach, $\phi(f)$ is assumed to be independent of frequency[1] (i.e. a constant) in the relevant detection range. This assumes damping introduced by Kimball and Lovell [*4*], which describes internal damping of mechanical structures, not including other damping, such as air resistance. Recall that we are interested in finding internal thermal noise.

The KAGRA mirror-suspension system is too complicated to solve for the value of $U_{\max}$ analytically, so this must be calculated numerically.

3.2 Energy calculation method

To find $U_{\max}$ numerically, the elastic deformation energy is calculated for the system under a simulation of the force applied. To find an expression that represents this energy, consider a

[1]Levin's method is capable of handling frequency-dependent ϕ values, but this will not be necessary for our work.

force creating a normal stress (say, in the x-direction), σ_x, on the cylinder. Suppose that this causes a strain of ϵ_x. Then there is a force of $\sigma_x \, dy \, dz$ acting over an extension of $\epsilon_x \, dx$.

Because the force and displacement have a linear relationship during loading, the work done by this force is

$$dU = \frac{1}{2}\sigma_x \epsilon_x \, dx \, dy \, dz \tag{10}$$

This analysis can be used for the other components of stress. This leads to five more terms of the form of Equation 10. It is assumed that there is no kinetic energy of the material in the maximally deformed state. The elastic deformation energy, then, is calculated with

$$dU = U_0 \, dx \, dy \, dz, \tag{11}$$

where the energy density, U_0, is defined as:

$$U_0 = \frac{1}{2}(\sigma_x \epsilon_x + \sigma_y \epsilon_y + \sigma_z \epsilon_z + \tau_{xy}\gamma_{xy} + \tau_{yz}\gamma_{yz} + \tau_{xz}\gamma_{xz}). \tag{12}$$

Here, σ and τ are normal and shear stress, and ϵ and γ are lateral and shear strain, respectively [5]. The components of the stress and strain tensors are numerical outputs, as is the volume integral of dU.

3.3 Energy verification

A simple calculation was performed to verify the accuracy of this method of calculating energy. A stiff rod was created in the finite-element software COMSOL Multiphysics 4.4, and the ends of the rod were pushed inward by a uniform pressure. The elastic potential energy in this rod was calculated, first with the method of Equations 11 and 12, and second using the integral of Hooke's law,

$$U = \frac{EA_0 \Delta L^2}{2L_0}. \tag{13}$$

Here, E is Young's modulus, A_0 is the rod's original cross-sectional area, L_0 is the original length of the rod, and ΔL is the change in the rod's length. The model used for this test is shown in Figure 1.

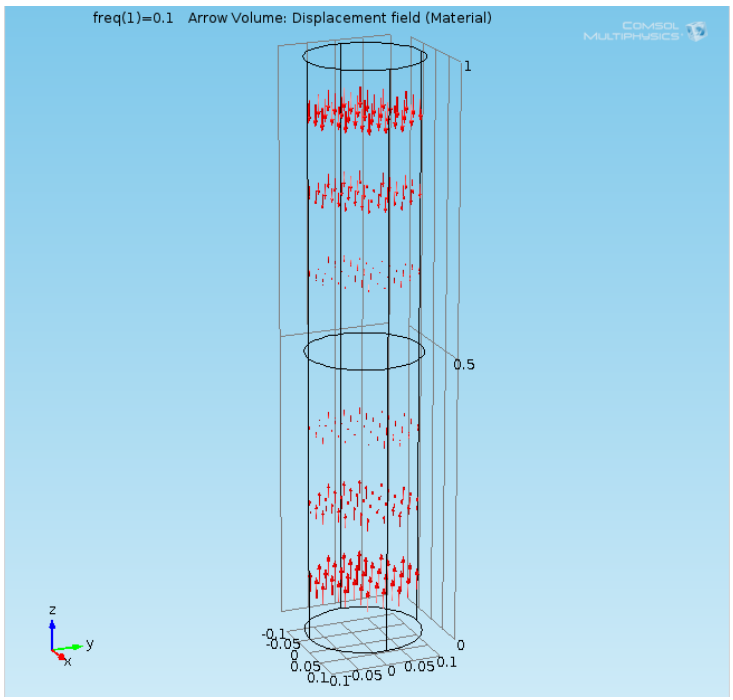

Figure 1: The model and displacement field for the rod energy test

In this test, the following numerical values were used: $E = 1 \times 10^7$ Pa, $L_0 = 1$ m, and a radius of 10 cm. The energy found with Equations 11 and 12 was 1.57041×10^{-5} J. The energy found with Equation 13 was 1.57057×10^{-5} J. These values agree within 0.01%.

3.4 Basic model

To develop the methods used for the mirror-suspension system and compare initial results, we calculate the thermal noise spectrum for a basic model: one cylindrical mirror with an incoming laser beam. Using COMSOL Multiphysics 4.4, we create a cylinder and apply a Gaussian load

to one face with a pressure of the form

$$P(\vec{r}) = F_0 f(\vec{r}), \tag{14}$$

with F_0 and $f(\vec{r})$ as defined in Equation 6; for a beam of radius r_0, $f(\vec{r})$ takes the form:

$$f(\vec{r}) = \frac{1}{\pi {r_0}^2} \mathrm{e}^{r^2/{r_0}^2}. \tag{15}$$

The cylinder is constrained when the force is applied. Specifically, the center of mass is fixed,

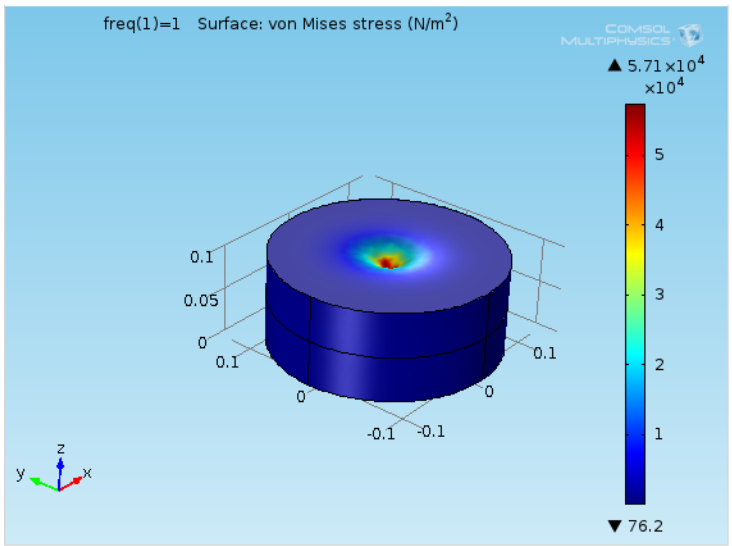

Figure 2: The model and von Mises stress caused by the Gaussian load

and rigid body rotations of the cylinder are disabled. This is not necessarily a safe way to measure the stresses and strains (the center of mass should have a small oscillation under such a load), but it is at the very least in accordance with others' results in order of magnitude.

This force is simulated (an image of the simulation is shown in Figure 2), and the stress and strain tensors calculated by COMSOL in local coordinates are used for these values. The resulting energy density is integrated over the volume to find $U_{\max}$.

In this calculation, the values used by Levin [*2*], as well as Gillespie and Raab [*6*], are used. These are: $r_0 = 1.56$ cm, $E_0 = 7.18 \times 10^{10}$ Pa, $\sigma = 0.16$, $\phi(f) = 10^{-7}$, a mirror diameter of 25 cm, and a mirror thickness of 10 cm.

The computed result for thermal noise density at 100 Hz is $S_x(100\text{Hz}) \simeq 5.90\times10^{-40}\text{m}^2/\text{Hz}$. Levin's work has found a value of $S_x(100\text{Hz}) \simeq 8.76 \times 10^{-40}\text{m}^2/\text{Hz}$. These values have the same order of magnitude despite the fixing of the center of mass, and this is sufficient for the estimations we are seeking.

3.5 Meshing verification

The results were compared when using various meshes: first, a physics-controlled mesh (using triangular meshing), and second, a symmetric mesh created with a mapped meshing on the face and a swept mesh along the body. These two meshes are shown in Figure 3. With the physics-controlled mesh, a spectrum of $S_x(f) = 5.8960 \times 10^{-40}\ \text{m}^2/\text{Hz}$ was calculated; with the symmetric mesh, a spectrum of $S_x(f) = 5.9019 \times 10^{-40}\ \text{m}^2/\text{Hz}$ was calculated. These converge to approximately the same value, independent of mesh. This is a necessary quality for the value calculated.

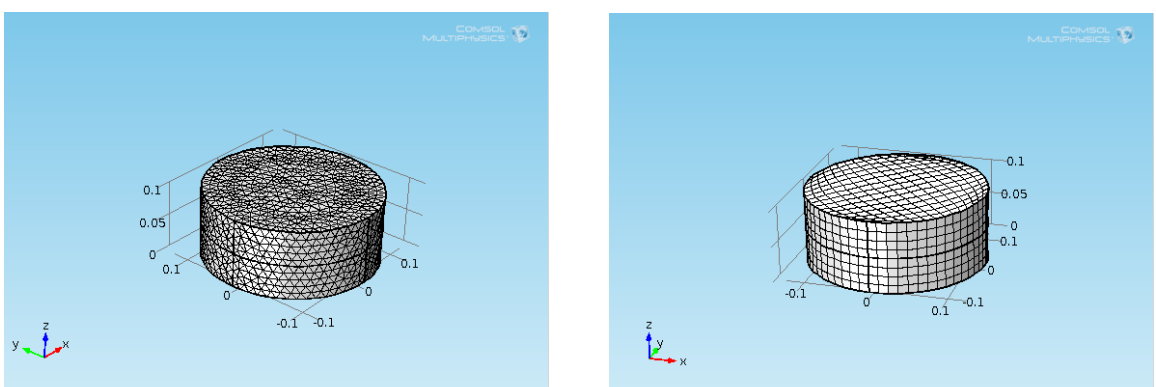

(a) Physics-controlled (b) Symmetric

Figure 3: The two meshes used to compare spectrum results

3.6 Cradle system model

One of the candidates for KAGRA's cryogenic suspension system involves a cradle design. Specifically, this is a body (in this case a rectangular prism) with a cavity in which the mirror

sits. There are two thin patches of adhesive between the cradle and the mirror. The mirror and cradle will be composed of sapphire,[2] and the thin adhesive is pure indium. This is a compromised design; it is useful in that it can be bonded properly and easily repaired or replaced. A model of the system is shown in Figure 4.

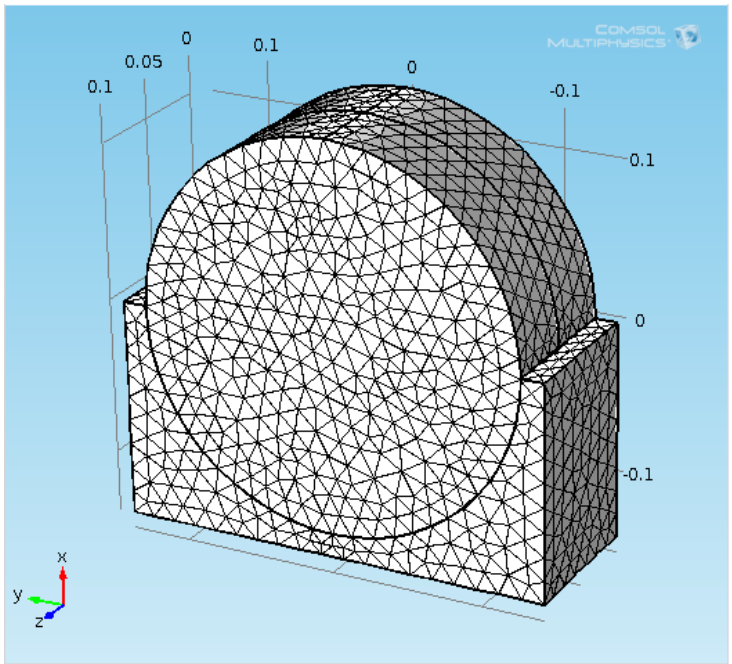

Figure 4: The model used for the cradle system

The mirror and cradle are both meshed with tetrahedral elements. The patches of indium have a triangular meshing across the wide surface, and this meshing is swept through the thin direction. The patches have a thickness of 100 nm, and the maximum mesh element size in this direction is 10 nm.

This system is analyzed with the same method as the basic model. One key difference, though, is that the loss factors differ between the sapphire mirror-cradle system and the indium patches. The thermal noise spectrum must be separated by adjusting Equation 9:

$$W_{\text{diss}} = 2\pi f (U_{\text{max, sapphire}}\, \phi_{\text{sapphire}}(f) + U_{\text{max, indium}}\, \phi_{\text{indium}}(f)). \tag{16}$$

[2]Sapphire is chosen for the mirrors because of its optical and thermal properties at cryogenic temperatures.

The values for $\phi_{\text{sapphire}}(f)$ and $\phi_{\text{indium}}(f)$ are assumed to be independent of frequency, as before. The values for each U_{max} term are found by integrating the dU term from Equation 11 over the respective domain.

The desired value for ϕ_{indium} is calculated using this method. It is preferable for the indium patches to add only insignificant thermal noise to the system; a value of 10% of the thermal noise spectrum generated by the mirror-cradle system is assigned for the limit of the thermal noise generated by the indium patches. The loss factor to fit this characteristic is calculated with the finite-element analysis results.

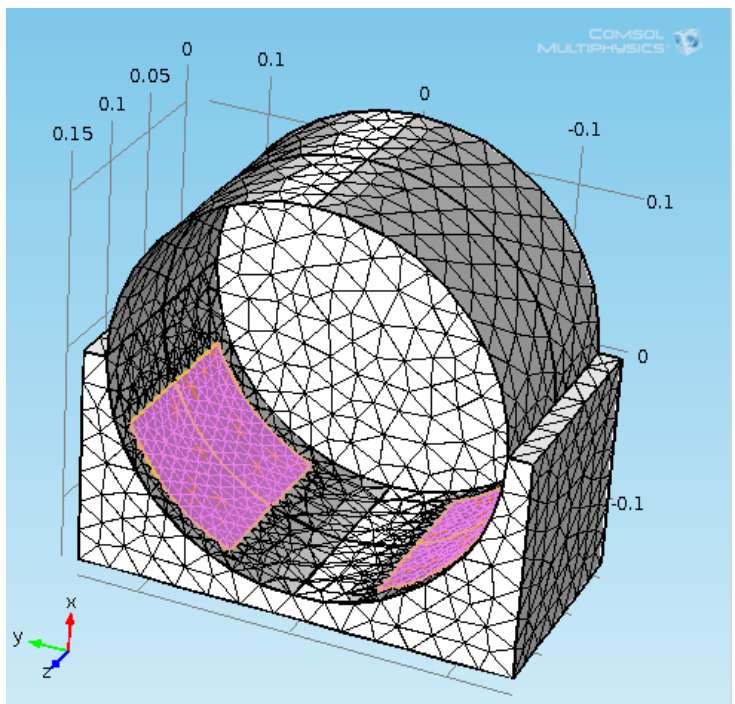

Figure 5: The indium patches are highlighted in purple (the front face has been hidden)

4 Results and discussion

The parameters and numerical values used in the finite element calculation are outlined below. The results for the loss factor calculation with the given values are displayed, as well.

4.1 Parameters

The parameters and the associated values used in this work are given in Table 1. In this table, E represents the respective Young's modulus, ν represents the respective Poisson's ratio, and ρ is the respective density. For sapphire, elastic stiffness constants are necessary since the material is anisotropic; these are represented with the C values, [7] corresponding to standard elastic stiffness constants.

Table 1: The parameters and values used in the cradle-mirror simulation

Parameter	Value
F_0	100 N
d_{mirror}	25 cm
l_{mirror}	15 cm
r_0	1.56 cm
T	20 K
f	100 Hz
w_{block}	28 cm
h_{block}	14 cm
E_{sapphire}	356.5 GPa
ν_{sapphire}	0.305
ρ_{sapphire}	3970 kg/m^3
ϕ_{sapphire}	1.56×10^{-7}
C_{11}	197.3 GPa
C_{33}	500.9 GPa
C_{44}	146.8 GPa
C_{12}	162.8 GPa
C_{13}	116.0 GPa
C_{14}	-21.90 GPa
E_{indium}	1.27 GPa
ν_{indium}	0.4498
ρ_{indium}	7310 kg/m^3
z_{indium}	100 nm
l_{indium}	12 cm
$\Delta\theta_{\text{indium}}$	45°
$\theta_{d,\text{indium}}$	45°

In the geometry, d represents the diameter of the mirror; l represents the thickness (perpen-

dicular to the mirror's surface); w and h represent the width and height of the cradle, respectively; z is the thickness of the indium patches, $\Delta\theta$ is the angle covered by each patch along the mirror's circumference; θ_d is the angle between the center of each patch and the vertical axis.

In the simulation, a force of the form of Equation 6 is applied to one face of the mirror, centered at the center of the mirror's face. This is done with a frequency domain study at 100 Hz. The calculation is done with ϕ_{indium} values of 10^{-5}, 10^{-4}, 0.001, 0.01, and 0.1.

4.2 Example loss factor calculation

At 100 Hz, the mirror-cradle system (not including the indium patches) generates a thermal noise density of $1.197\times10^{-41}\mathrm{m}^2/\mathrm{Hz}$. This is not a function of indium's loss factor (see Equation 16), so this remains constant when adjusting the loss factor.

The values for thermal noise density as a function of indium's loss factor is shown in Figure 6, and the values are given in Table 2. This is a linear function, as can be seen in Equation 9's linear dependence on ϕ.

Table 2: The total displacement thermal noise density spectrum calculated for each indium loss factor at 100 Hz.

ϕ_{indium}	$S_{x,\,\text{total}}$(100 Hz)
10^{-5}	1.2078×10^{-41}
10^{-4}	1.3052×10^{-41}
0.001	2.2785×10^{-41}
0.01	1.2012×10^{-40}
0.1	1.0935×10^{-39}

The results of Figure 6 can be described by an equation of approximately

$$S_{x,\text{total}} = (1.082 \times 10^{-38}\phi_{\text{indium}} + 1.197 \times 10^{-41})\,\mathrm{m}^2/\mathrm{Hz} \tag{17}$$

For the thermal noise density to reach a value of no more than 10% higher than $1.197 \times 10^{-41}\mathrm{m}^2/\mathrm{Hz}$ (of the mirror and cradle alone), the loss factor for indium must be approximately $\phi_{\text{indium}} = 1.1 \times 10^{-4}$.

This value is based on arbitrary conditions chosen for the simulation. However, this gives an idea of the qualities necessary in the indium patches. More importantly, this simulation technique can be used in future iterations with other proposed designs to calculate various properties of the system's internal thermal noise.

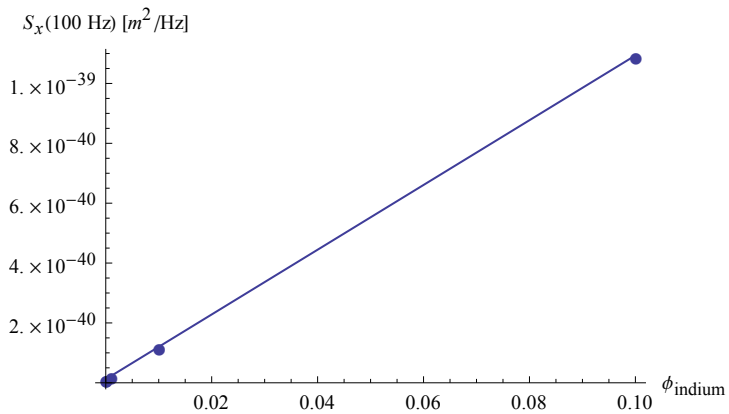

Figure 6: A plot of total internal displacement thermal noise spectral density $(\mathrm{m}^2/\mathrm{Hz})$ vs. loss factor at 100 Hz

5 Acknowledgments

This work would not have been possible without the frequent guidance of Yoichi Aso and Raffaele Flaminio. Resources were provided by the National Astronomical Observatory of Japan, as well as the University of Florida's International REU program, a National Science Foundation initiative.

6 References

1. H. B. Callen, T. A. Welton, *Phys. Rev.* **83**, 34 (1951).

2. Y. Levin, *Phys. Rev. D* **57**, 659 (1998).

3. C. Wipf, Toward quantum opto-mechanics in a gram-scale suspended mirror interferometer, Ph.D. thesis, MIT (2013).

4. A. L. Kimball, D. E. Lovell, *Phys. Rev.* **30**, 948 (1927).

5. S. P. Timoshenko, J. N. Goodier, *Theory of Elasticity* (McGraw-Hill Book Company, 1970), p. 245.

6. A. Gillespie, F. Raab, *Phys. Rev. D* **52**, 577 (1995).

7. T. Goto, O. L. Anderson, I. Ohno, S. Yamamoto, *Journal of Geophysical Research: Solid Earth* **94**, 7588 (1989).

8. P. R. Saulson, *Phys. Rev. D* **42**, 2437 (1990).

9. L. D. Landau, E. M. Lifshitz, *Theory of Elasticity* (Elsevier Ltd., 1986), third edn.

10. G. Harry, T. P. Bodiya, R. DeSalvo, eds., *Optical Coatings and Thermal Noise in Precision Measurement* (Cambridge University Press, 2012).

11. G. I. Gonzlez, P. R. Saulson, *The Journal of the Acoustical Society of America* **96** (1994).

12. C. Kittel, *Introduction to Solid State Physics* (John Wiley & Sons, Inc., 2005), 8th edn.

13. T. Vodenitcharova, *et al.*, *Journal of Materials Processing Technology* **194**, 52 (2007).

14. I. Babuška, J. R. Whiteman, T. Strouboulis, *Finite Elements: An Introduction to the Method and Error Estimation* (Oxford University Press, 2011).

15. R. W. Pryor, *Multiphysics Modeling Using COMSOL 4: A First Principles Approach* (Mercury Learning and Information LLC, 2012).